THE ASTROPHYSICAL JOURNAL, 404:112–123, 1993 February 10

THE X-RAY SPECTRAL VARIABILITY OF THE BL LACERTAE TYPE OBJECT PKS 2155−304

S. SEMBAY AND R. S. WARWICK
Department of Physics and Astronomy, University of Leicester, University Road, Leicester LE1 7RH, UK
C. MEGAN URRY AND J. SOKOLOSKI
Space Telescope Science Institute, 3700 San Martin Drive, Baltimore, MD 21218
I. M. GEORGE
HEASARC, Code 668, NASA/Goddard Space Flight Center, Greenbelt, MD 20771
F. MAKINO
Institute of Space and Astronautical Science, 3-1-1, Yoshinadai, Sagamihara, Kanagawa 229, Japan
AND
T. OHASHI AND M. TASHIRO
Department of Physics, University of Tokyo, 3-1, Hongo 7-chome, Bunkyo-ku, Tokyo 113, Japan
Received 1992 May 20; accepted 1992 August 11

ABSTRACT

We present a detailed study of the hard X-ray properties of the BL Lacertae object PKS 2155−304 based on measurements made in 1988 and 1989 with the Large Area Counter (LAC) on board the *Ginga* satellite. The source exhibited a high degree of variability with a dynamic range of a factor 7 in the 2–6 keV band. The fastest amplitude variation was a factor 2 decline in the intensity in this band within 4 hours. The spectrum is characterized by a break which occurs at ∼4 keV. Spectral fits to the data integrated in 6400 s time bins reveal that, in common with previous observations of BL Lacertae objects, the spectral slope is generally anti-correlated with intensity in the sense that the spectrum hardens as the intensity increases. However, the tracks of sequential points in the index-intensity plane are occasionally seen to differ during the rise and decay stages of individual flares. Furthermore, during one, or possibly two, flaring episodes the spectral index is observed to *correlate* with intensity variations. The X-ray properties of PKS 2155−304 are most readily interpreted in terms of direct synchrotron radiation originating within a relativistic jet, however, the X-ray emitting region is probably more complex than the geometries assumed in most standard jet models. Further development of time-dependent theoretical models will be necessary to explain some of the details of the present observations.

Subject headings: BL Lacertae objects: individual: (PKS 2155−304) — radiation mechanisms: cyclotron and synchrotron — X-rays: galaxies

1. INTRODUCTION

Flux and spectral variability provide two of the most powerful diagnostics in the study of active galactic nuclei (AGNs). The hypothesis that the power emission from AGNs is ultimately derived from a compact region, or central engine, smaller than our own solar system, is largely built upon observations of short time scale variability and the inferred light crossing times. In many blazars (BL Lacertae objects and OVV quasars) the variability can be so rapid that the theoretical maximum efficiency limit for isotropic emission is exceeded and relativistic beaming must be invoked (Blandford & Rees 1978). In turn spectral variability can provide an important insight into the physics of the emission mechanisms and the distribution of matter around the central engine.

PKS 2155−304 is one of the brightest and most variable BL Lac objects known. It was the first discovered as an X-ray source by the *HEAO 1* satellite (Schwartz et al. 1979; Griffiths et al. 1979) and later identified with an optical counterpart showing the featureless continuum and polarization typical of the BL Lacertae class (Schwartz et al. 1979). Bowyer et al. (1984) detected the presence of weak absorption features from a stellar population at a redshift of $z = 0.117$ in a faint nebulosity associated with the optical candidate. However, recent results from optical CCD observations have shown that the nebulosity can be resolved into an extended symmetric structure consistent with that of an elliptical galaxy plus a faint companion galaxy located ∼4″.5 from the nucleus (Falomo, Melnick, & Tanzi 1990). Falomo et al. (1991) have now established that the absorption features in fact arise from the companion and derive a redshift for the BL Lac of $z = 0.08$–0.13 based on the absolute-magnitude effective radius relation for luminous elliptical galaxies. If the host galaxy of PKS 2155−304 has an absolute magnitude typical of other BL Lac objects then $z \simeq 0.1$ and we have adopted this value in the present work.

Variability in the continuum emission from PKS 2155−304 has been observed in the optical (Carini & Miller 1992), ultraviolet (Maraschi et al. 1986; Edelson et al. 1991; Urry et al. 1992) and X-ray (Urry, Mushotzky, & Holt 1986; Morini et al. 1986) bands with the largest dynamic range and most rapid variability apparent at the highest energies. The X-ray luminosity typically ranges over a factor of 10, with a factor of 4 increases in a time scale as short as 4 hours observed on one occasion by *EXOSAT* (Morini et al. 1986).

PKS 2155−304 has a steep hard X-ray spectrum with energy index typically in the range $1.5 \lesssim \alpha \lesssim 2.5$ (e.g., Urry et al. 1986). Simultaneous ultraviolet and X-ray observations by the *International Ultraviolet Explorer* (*IUE*) and *EXOSAT* show that the extrapolated hard X-ray continuum appears to extend down to the soft X-ray band and then flattens by $\Delta\alpha \sim 1.0$ to connect up with the ultraviolet (Treves et al. 1989). Recent results from a short observation by the Broad Band

X-ray Telescope (BBXRT) indicate a further break in the spectrum around 2.0 to 4.0 keV (Madejski et al. 1991). The gradual steepening of the continuum from the optical to the X-ray band in this and other BL Lac objects is commonly interpreted in terms of inhomogeneous synchrotron self-Compton (SSC) models. In this context a hard tail above 10 keV seen by *HEAO 1* (Urry & Mushotzky 1982) was identified as the self-Compton component of the lower energy synchrotron emission; however, the presence of this feature has not been confirmed by *EXOSAT* or *Ginga* (Ohashi et al. 1989).

A deep absorption feature at 0.6–0.7 keV was detected by the objective grating spectrometer (OGS) on the *Einstein Observatory* (Canizares & Kruper 1984). Assuming a redshift of $z \simeq 0.1$ the most likely interpretation for this feature is an O VIII Lyα resonance absorption trough associated with hot gas with an outflow velocity of $\sim 30{,}000$ km s^{-1} (Canizares & Kruper 1984; Krolik et al. 1985). The OGS spectrum has a very steep slope ($\alpha_{sx} \sim 5.0$) between 300 and 600 eV which is evidence for the presence of a soft excess. Wandel & Urry (1991) have suggested that the soft excess may arise from thermal radiation and have fitted the OGS spectrum and a contemporaneous *IUE* spectrum with an accretion disk model.

In this paper we present the results of four X-ray observations of the BL Lacertae object PKS 2155−304 performed by the *Ginga* satellite during 1988–1989. The X-ray data are presented in § 2. Light curves are shown for each epoch and spectral fits to the data are described. The behavior of the spectral slope with changes in intensity is also investigated. In § 3 we compare the observed X-ray properties with published contemporaneous optical and ultraviolet observations. In the final section we discuss the observations with reference to current models for the continuum emission from BL Lac objects.

2. X-RAY OBSERVATIONS

2.1. *Observation Log and Background Subtraction*

PKS 2155−304 was observed by the *Ginga* LAC (Turner et al. 1989) once in 1988 and three times in 1989. An earlier observation of the source by *Ginga* made in 1987 has been reported by Ohashi et al. (1989). A summary of the observation log including the on-source exposure times and observed count rate ranges is given in Table 1. The on-source exposure during a given observation is limited mainly by Earth occultation and passage of the satellite through high background regions. In the latter phase of the *Ginga* mission there was a tendency for the satellite pointing direction to drift during an observation. In the present analysis we have only used data for which the pointing offset was less than 0°.5. Since for large angles one must apply a correction factor to the observed flux which is dependent on both the offset angle and energy, this conservative limit avoids the possibility of introducing spurius spectral variations as a function of time. This procedure resulted in some loss of data during the observations in 1989.

TABLE 1

LOG *GINGA* OBSERVATIONS OF PKS 2155−304

Start Date (UT)	Duration (s)	Exposure (s)	Count Rate (2–10 keV) (count s^{-1})
1988 May 12 19:50:00	80128	30200.2	12–23
1989 Oct 02 18:45:40	134976	46811.6	80–102
1989 Oct 10 09:45:13	171200	67338.2	27–46
1989 Oct 24 01:12:07	146432	22913.7	37–55

The LAC background can be estimated in one of two ways. The "local" method (Method I of Hayashida et al. 1989), requires a background observation of about 24 hours duration either immediately before or after the source observation. The background during the on-source observation can then be estimated from a model which incorporates the expected count rates due to a variety of processes including the internal detector background, the diffuse X-ray background (XRB), and time-dependent radioactive activation of the satellite after passages through the radiation belts. The "universal" method (Method II of Hayashida et al. 1989) enables the background during an on-source observation to be predicted from a series of background observations spread over a period of a few months. An advantage of this method is that the background includes a model of the 37 day periodicity which arises due to the variation in the altitude at which the satellite passes through the South Atlantic Anomaly (SAA). The method does not, however, provide any corrections for possible variations in the Galactic diffuse XRB or temporal changes in the in-orbit radiation environment. For consistency we have employed the universal background-subtraction method throughout this work as most of the observations during 1989 lacked suitable local background observations. A comparison of the result from observations in which both background subtraction methods were used revealed no significant differences. The systematic uncertainty in the background subtraction is quite stable in the sense that the expected residual error is fairly constant over a time scale of 24 hr. The absolute magnitude of the error ranges from ~ 0.04 counts s^{-1} keV^{-1} at 2 keV to better than ~ 0.02 counts s^{-1} keV^{-1} above 10 keV.

2.2. *Light Curves and Hardness Ratios*

Background-subtracted light curves, in the energy range 1.7–5.8 keV (LAC channels 4–10, channels 1–3 are not used in the analysis), are shown in Figures 1*a*, 2*a*, 3*a*, and 4*a*. The data have been binned at 1280 s resolution. The extreme variability of PKS 2155−304 in the X-ray regime is clearly apparent. Compared to the low state of the source observed in 1988 May 12, the source was 7 times brighter in 1989 October 2/3. Eight days later in 1989 October 10/11 the source had dimmed by a factor of ~ 2.5. It then brightened again two weeks later in 1989 October 24/25. Short time scale variability within each observation is evident with the most rapid change being a drop by a factor of 2 in intensity within 4 hours on 1989 October 10, this is comparable to the most rapid flux doubling times previously observed (Morini et al. 1986). There appears to be no obvious systematic difference between the time scales for the rise and decay phases of each outburst.

Tagliaferri et al. (1991) have inferred variability time scales as short as 300–400 s by employing power spectrum analysis techniques on *EXOSAT* data. A similar search for short time scale variability within the present *Ginga* data is complicated by the numerous data gaps within the time series, and discussion of such results are postponed to a future paper.

In Figures 1*b*, 2*b*, 3*b*, and 4*b* we show the hardness ratio, defined as the LAC count rate in the 5.8–15.2 keV band divided by that in the 1.7–5.8 keV band, for each observation as a function of time. It can be seen that the hardness ratio is also highly variable, with the overall trend between observations being such that the X-ray spectrum is hardest when the source is brightest. This is a common property of BL Lac type

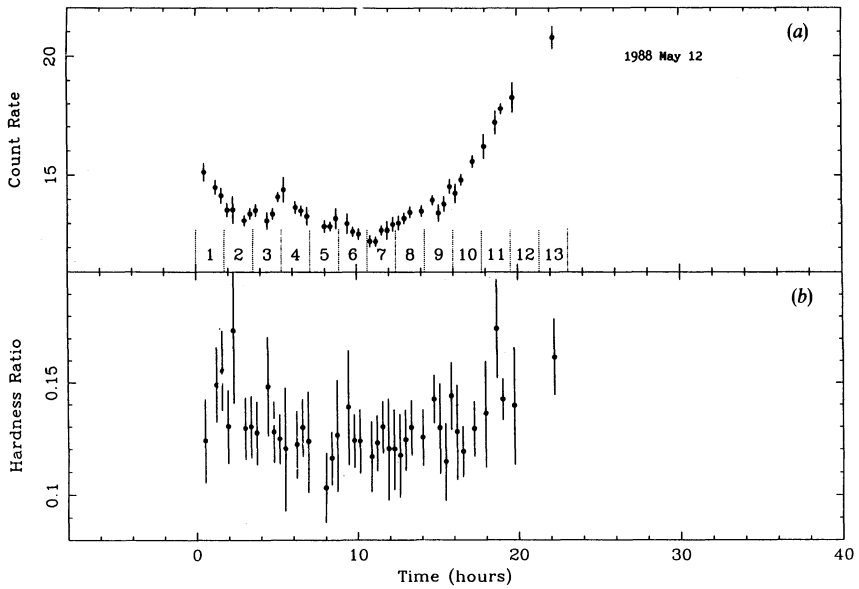

FIG. 1.—(*a*) 1.7–5.8 keV count rate (counts s^{-1}). 0 hours on the time axis is at UT = $19^h50^m00^s$, 1988 May 12. (*b*) Hardness ratio defined as the ratio of the 5.8–15.2 keV count rate to the 1.7–5.8 keV count rate.

objects (e.g., George, Warwick, & Bromage 1988; Giommi et al. 1990). On time scales of a few hours, a positive correlation between hardness ratio and flux is observed during the 1988 May 12 observation, the second flare of the 1989 October 2 observation and the second and third flares of the 1989 October 10 observation. During the first flare of the 1989 October 2 observation and possibly at the beginning of the 1989 October 24 observation there are episodes of an anti-correlation between hardness and flux. This is the first time such behavior has been observed in the X-ray spectra of a BL Lac object, and will be discussed more fully below.

2.3. *Spectral Analysis*

A spectral analysis of the time-averaged PHA data was performed using 6400 s bins. The integration time was chosen such that it provided adequate statistical accuracy during the low-intensity states, but was still short enough to be representative of the observed flux variability time scale. For convenience, the actual time bins used are delineated by the dotted short vertical lines in Figures 1*a*, 2*a*, 3*a*, and 4*a*. The energy range was restricted to 1.7 to 17.9 keV (29 energy bins), the upper bound being the maximum energy at which a statistically significant count rate was detected when the source was weakest.

The recent observation of PKS 2155−304 by BBXRT revealed an intrinsic steepening of the spectrum above 2.0 to 4.0 keV and a low energy absorption consistent with the Galactic neutral hydrogen column density of $\sim 1.8 \times 10^{20}$ cm^{-2}. A model consisting of a single power law plus low energy absorption fixed at the Galactic value (assuming cosmic

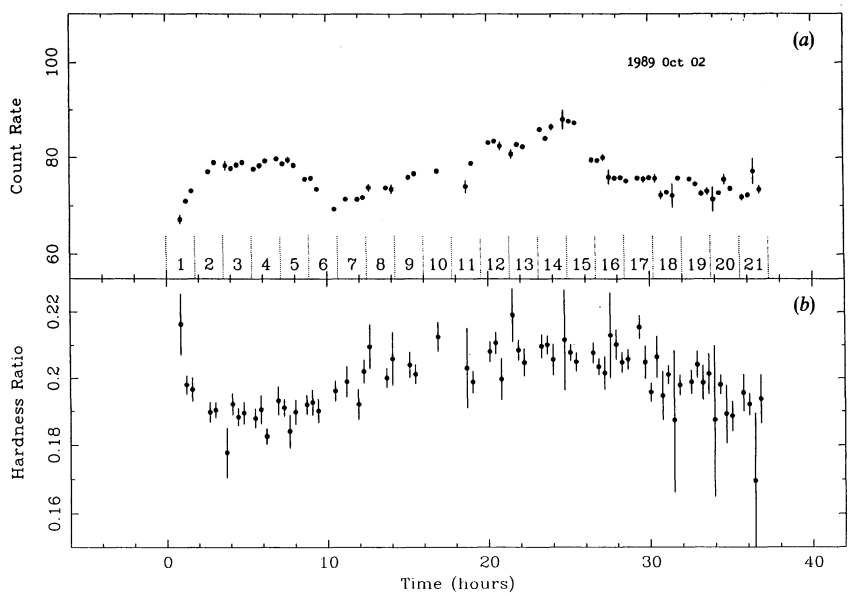

FIG. 2.—Same as Fig. 1, except 0 hours on the time axis is at UT = $18^h45^m40^s$, 1989 October 2

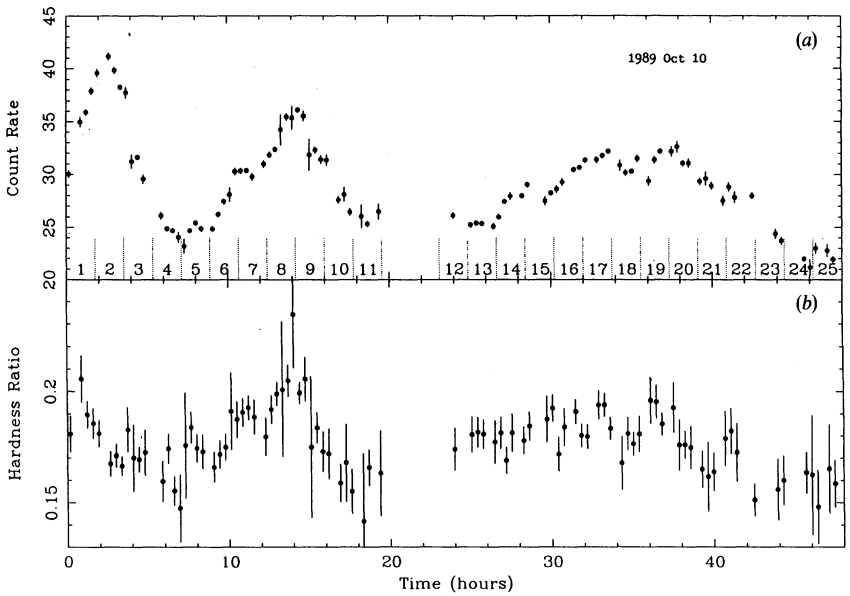

FIG. 3.—Same as Fig. 1, except 0 hours on the time axis is at UT = $09^h45^m13^s$, 1989 October 10

abundances and absorption cross sections given in Morrison & McCammon 1983) gave a very poor fit to the *Ginga* data with the minimum χ^2_ν exceeding the 95% acceptance level of 1.48 for 27 degrees of freedom in about two-thirds of the 73 spectral fits. Hence, we have used a spectral model consisting of a broken power law with the column density fixed at the Galactic value. This model gave statistically acceptable minimum χ^2_ν-values in each of the fits. In Figures 5*a*–5*c* we have plotted the best-fit values of the low- and high-energy spectral indices and the energy of the spectral break, in the rest frame of the source, against the 2–10 keV source flux corrected for intrinsic absorption. Whereas there is a significant correlation between the spectral indices and the source intensity, in the sense that the slope is generally harder when the source is brighter, there is no apparent correlation between the energy of the spectral break and the intensity. The mean value of the break energy was found to be 3.8 ± 0.2 keV. The low energy spectral index is typically less well constrained than the high-energy index simply because the break occurs within the first three or four significant PHA channels.

We then repeated the spectral analysis with the energy of the spectral break fixed at its mean value. Again, in each case, the fits gave acceptable values of χ^2_ν with no statistically significant differences in comparison with the previous fits. In Figure 6 we have plotted the spectral index in the range 1.7 to 3.8 keV ($\alpha_{1.7-3.8}$) against the index in the range 3.8 to 17.9 keV ($\alpha_{3.8-17.9}$). The error bars are the 68% confidence intervals calculated assuming two parameters of interest ($\alpha_{1.7-3.8}$ and $\alpha_{3.8-17.9}$; $\Delta\chi^2 = 2.3$). Apart from two points from fits to low significance data the higher energy index is systematically

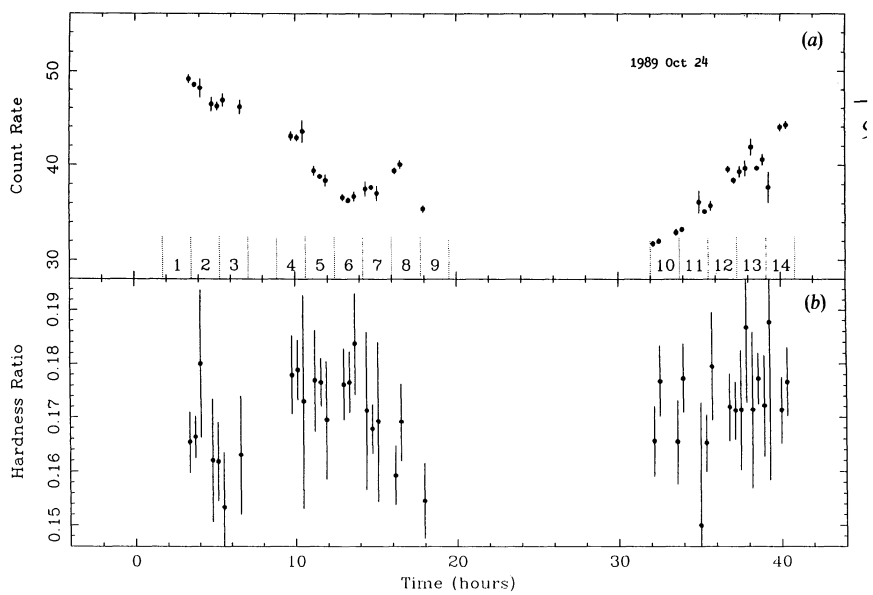

FIG. 4.—Same as Fig. 1, except 0 hours on the time axis is at UT = $01^h12^m07^s$, 1989 October 24

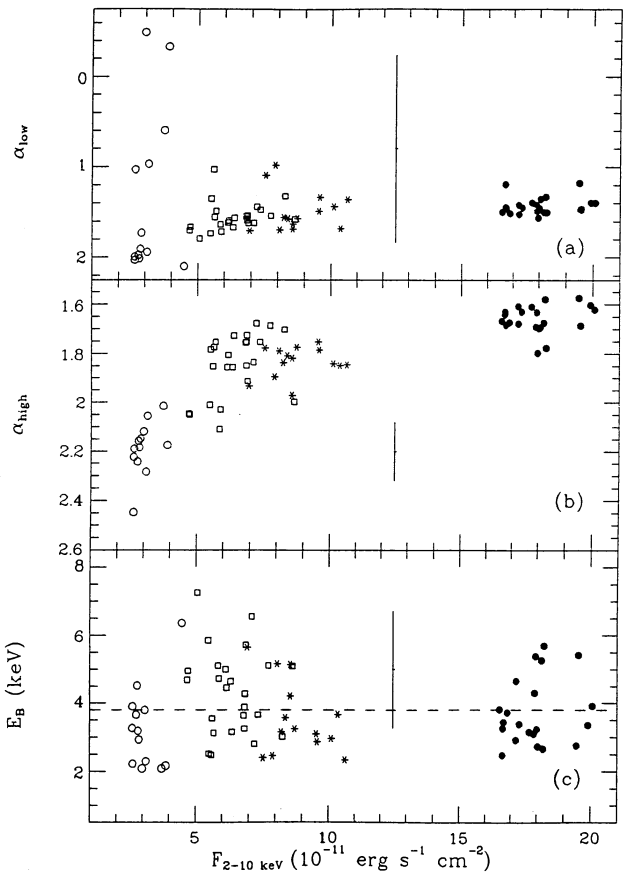

FIG. 5.—Result of broken power-law fits to the data integrated at 6400 s resolution: (*a*) low-energy spectral index, (*b*) high-energy spectral index and (*c*) break energy (keV). The mean break energy is shown by the dashed line. Error bars have been suppressed for clarity, however, the mean 68% confidence intervals are shown in each panel. Symbols designate (*open circles*) 1988 May 12 data, (*filled circles*) 1989 October 2 data, (*open squares*) 1989 October 10 data, and (*asterisks*) 1989 October 24 data.

steeper by $\Delta\alpha \sim 0.2$ indicating that the degree of curvature of the spectrum is constant.

These results indicate that within the range 1.7 to 17.9 keV the resolution of the *Ginga* data are such that the integrated 6400 s spectra can be parameterized with a model consisting of only two free parameters; the source intensity and the high-energy spectral slope. Hence, in order to more closely examine the relation between spectral slope and source intensity we refitted the data with the broken power-law model but fixed the break energy at 3.8 keV and the lower energy index, $\alpha_{1.7-3.8} = \alpha_{3.8-17.9} - 0.2$. In only three cases out of 73 spectral fits did the minimum χ^2_ν exceed the 95% acceptance level (1.48 for 27 degrees of freedom) as expected for a normal χ^2_ν distribution.

Excellent fits to the *Ginga* data can also be achieved by a single power law plus neutral absorbing column model if the column density parameter is allowed to vary. The consequence of the intrinsic spectral steepening is that the best-fit apparent column density typically has a value around $\sim 3 \times 10^{21}$ cm^{-2} which is significantly greater than the Galactic value. It is interesting to note that a similar result was obtained by Treves et al. (1989) in fits to *EXOSAT* ME data of the source. The derived spectral indices are consistent with the high-energy indices found in the broken power-law fits. The apparent column density is not correlated with the source intensity which leads to the same conclusion as before that the degree of curvature of the spectrum is constant.

In Figures 7*a*–7*e* we have plotted the energy index $\alpha_{3.8-17.9}$ from the two parameter broken power-law fit, versus the observed 2–10 keV source flux for each observation. Each point is numbered sequentially in time order (see Figs. 1*a*, 2*a*, 3*a*, and 4*a*) and, as a further aid to clarity, points are marked with solid and open symbols during intensity increases and decreases, respectively. The data from 1989 October 10/11 has been subdivided; Figure 7*c* follows the first two rapid flares and Figure 7*d* follows the third, longer, flare (see Fig. 3*a*).

The overall behavior of PKS 2155−304 during each of the observations is briefly summarized below:

1988 May 12.—The source is in its lowest intensity state during this observation. During the gradual decay from time bins 1 to 7 (Fig. 1), the index softens from $\alpha \simeq 2.1$ to $\alpha \simeq 2.3$ then hardens again as the source brightens. The error bars are large in the last two bins due to the relatively low exposure.

1989 October 2.—The source is seen in its highest state during this observation. Two distinct types of spectral behavior are apparent. During the first flare the index softens (with $\Delta\alpha \simeq 0.05$) in the rapid rise (bin 1 to 2), remains about constant with $\alpha \simeq 1.73$ during the flat section of the flare, then hardens again as the source decays back to near its original level (at bin 7). The spectral shape of the soft flare is discussed in § 2.4. In the second, longer, flare from time bins 7 to 21 the index is anticorrelated with flux following a single well defined track in the index-flux parameter space with ($\Delta\alpha \simeq 0.08$). The changes in spectral slope are small but quite significant because the high-intensity state of the source allows the spectral parameters to be derived with good accuracy.

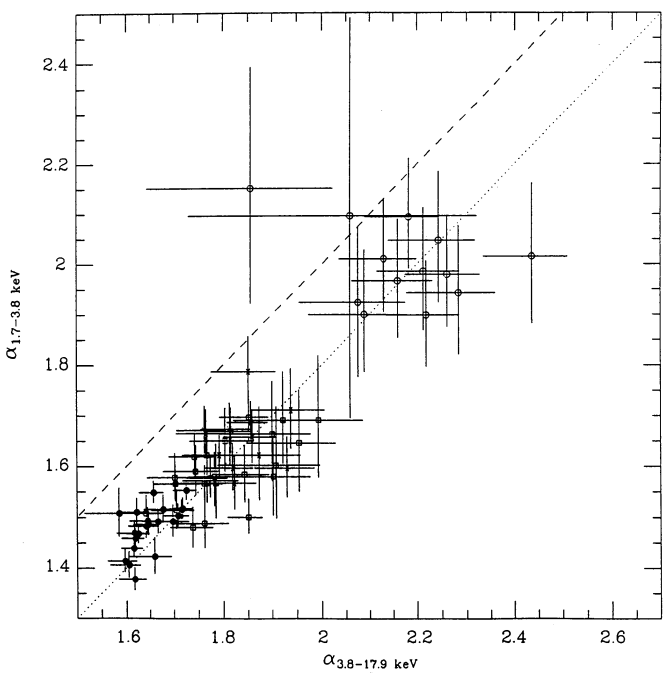

FIG. 6.—Best-fit energy index in the range 1.7–3.8 keV plotted against the energy index in the range 3.8–17.9 keV for the broken power-law fits. The error bars are the 68% confidence intervals assuming two parameters of interest in the fits. The higher energy index is systematically steeper than the lower energy index by $\Delta\alpha \sim 0.2$ apart from two fits to low significance data (last two bins of the 1988 May 12 observation). Symbols are as in Fig. 5.

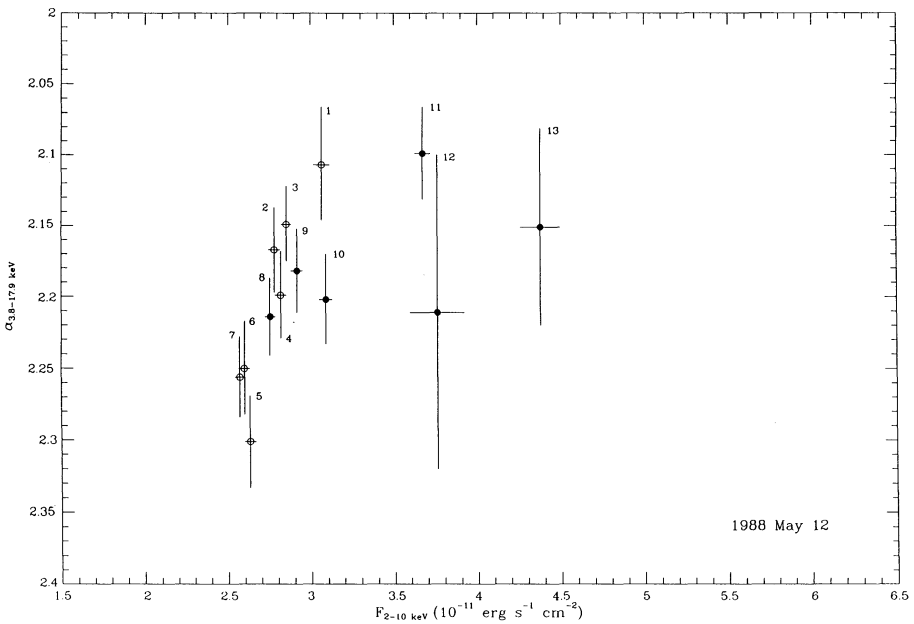

FIG. 7*a*

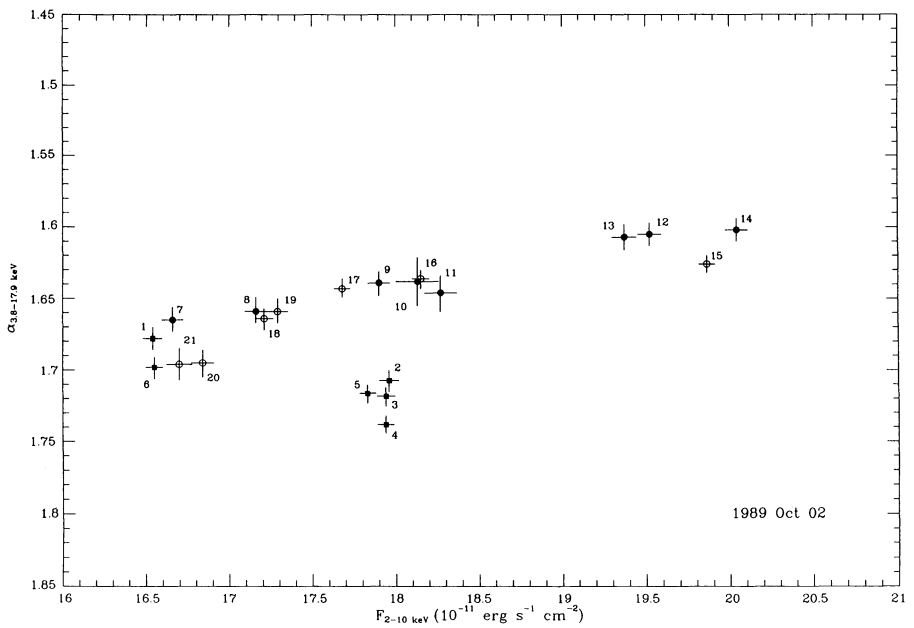

FIG. 7*b*

FIG. 7.—(*a*) Energy index in the range 3.8–17.9 keV vs. 2–10 keV flux (two free parameter fits) for the 1988 May 12 data. (*b*) Energy index in the range 3.8–17.9 keV vs. 2–10 keV flux (two free parameter fits) for the 1989 October 2 data. (*c*) Energy index in the range 3.8–17.9 keV vs. 2–10 keV flux (two free parameter fits) for the 1989 October 10 data. (*d*) Energy index in the range 3.8–17.9 keV vs. 2–10 keV flux (two free parameter fits) for the 1989 October 11 data. (*e*) Energy index in the range 3.8–17.9 keV vs. 2–10 keV flux (two free paramater fits) for the 1989 October 24 data.

1989 October 10.—The index is anticorrelated with flux during the two rapid flares from time bins 1 to 11 (Fig. 3) over a range $\Delta\alpha \simeq 0.3$. The rise and decay phases follow different tracks; the index following a clockwise or "hysteresis-like" loop in parameter space with time.

1989 October 11.—The index again follows a clockwise loop during this flare from time bins 12 to 25, but the track has a somewhat different "shape" than that for the flare on the preceeding day. The index changes little in rising phase then softens dramatically by $\Delta\alpha \simeq 0.2$ during the decay.

1989 October 24.—This observation shows a second episode of the anomalous index-flux correlation. In the first half of the decay (time bins 1 to 4) the index significantly hardens ($\Delta\alpha \simeq 0.2$). Then, during the rest of the decay and subsequent rise, the relation switches back to the more usual index-flux anticorrelation although with a very weak dependence. This

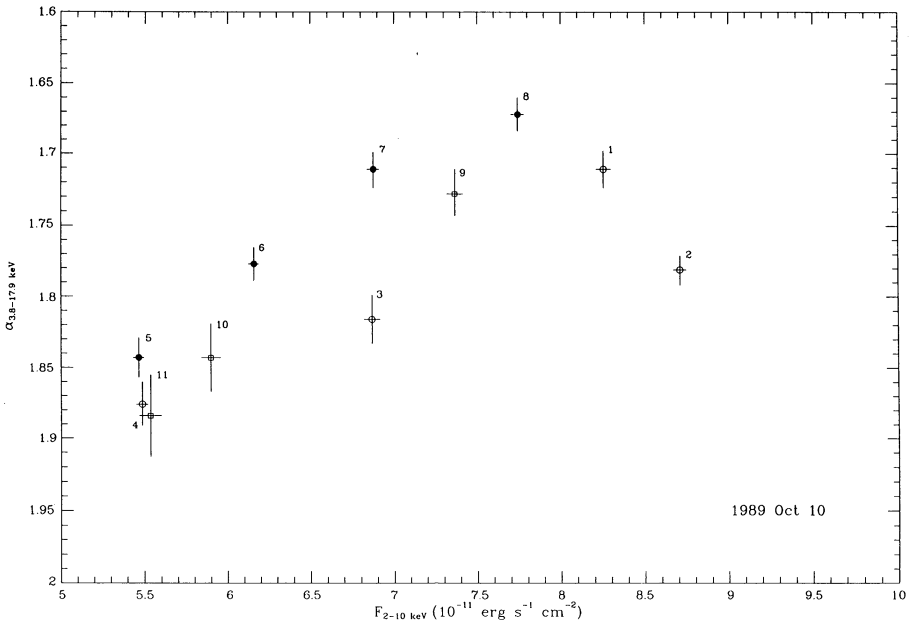

FIG. 7c

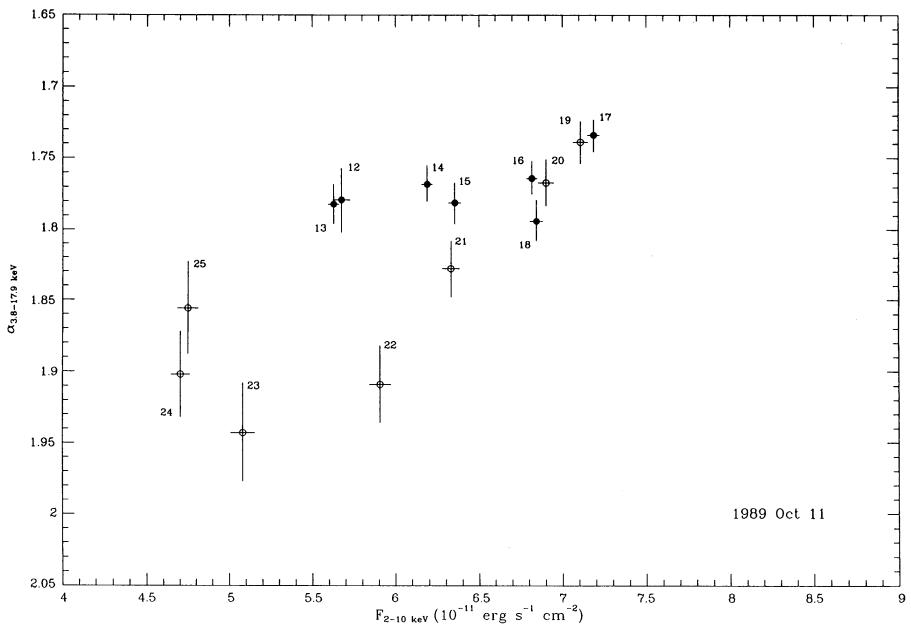

FIG. 7d

latter behavior is somewhat similar to that observed during the 1987 May *Ginga* observation reported by Ohashi et al. (1989) in which there was no apparent correlation of index and flux.

2.4. *Spectral Features*

2.4.1. *1989 October 2 Soft Flare*

We have investigated the spectral shape of the soft flare event observed in the 1989 October 2 data by subtracting the integrated spectrum from time bins 1, 6, and 7 from the integrated spectrum from time bins 2 to 5. The residual spectrum contains significant counts in the PHA channels up to about 12 keV and the observed 2 to 10 keV flux is $\sim 1.3 \times 10^{-11}$ ergs s^{-1} cm^{-2}. The results of fits to the residual spectrum with a variety of models are listed in Table 2. With each model the column density was fixed at the Galactic value. The best fit was achieved with a broken power law although a thermal Bremsstrahlung model also gives an acceptable minimum χ^2_ν-value. The higher energy section of the residual spectrum has a very steep slope and there is an abrupt break between the low- and high-energy slopes with $\Delta\alpha \sim 2$.

There is no known flaring X-ray source close enough to PKS 2155−304 to account for this event, however, we cannot exclude the possibility that it is a serendipitous source. One possible origin is that there may be an unknown UV Ceti-type flare star (late K and M dwarf stars) within the *Ginga* field of view. The temperature, intensity and duration of the event is

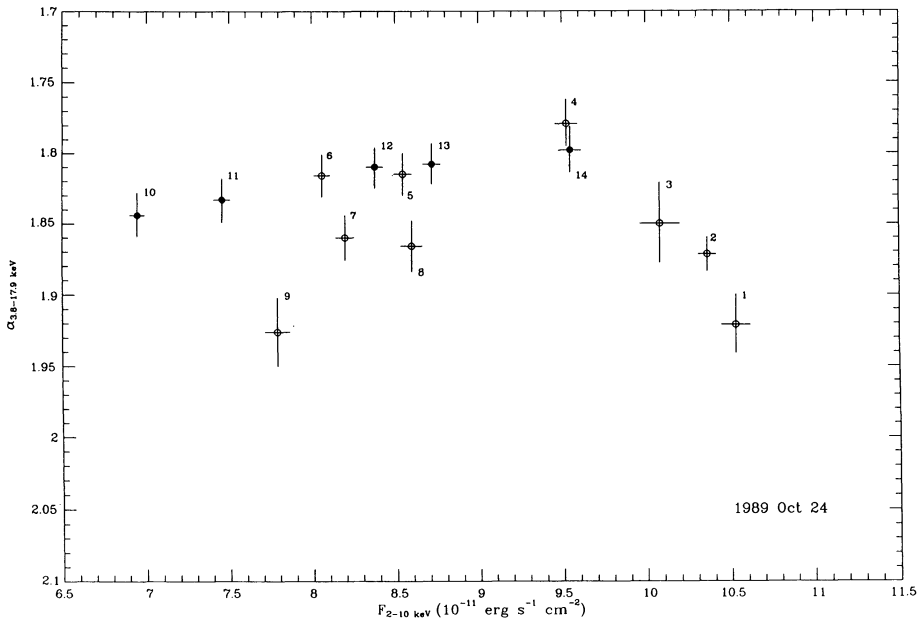

FIG. 7*e*

not untypical of the X-ray flares from these objects (e.g., Pallavicini, Tagliaferri, & Stella 1990). The peak flux of a flare can be an order of magnitude greater than the quiescent flux from the stars and there are four unidentified X-ray sources detected by the *EXOSAT* CMA within 0°.5 of the position of PKS 2155−304 (see ESA TM-12, 1991) with fluxes typically two orders of magnitude lower than PKS 2155−304 in this band. However, the occurrence rate of flares from these objects is typically one flare every ~10 hours (although with a wide dispersion) and it seems unlikely that given the large number of imaging observations of the PKS 2155−304 field by the *EXOSAT* CMA and the *Einstein* IPC that such an object would have remained undetected.

TABLE 2

SPECTRAL FITS TO 1989 OCTOBER 2 SOFT FLARE

Parameter	Value
Single Power Law ($z = 0.1$)	
α	$2.03^{+0.07}_{-0.07}$
χ^2_ν	1.90 (17 dof)
Broken Power Law ($z = 0.1$)	
α_{low}	$1.78^{+0.19}_{-0.22}$
α_{high}	$3.7^{+2.2}_{-1.1}$
E_b (keV)	$5.4^{+1.1}_{-1.0}$
χ^2_ν	1.16 (15 dof)
Bremsstrahlung ($z = 0.1$)	
kT_e (keV)	$2.43^{+0.14}_{-0.13}$
χ^2_ν	1.24 (17 dof)
Bremsstrahlung ($z = 0.0$)	
kT_e (keV)	$2.21^{+0.13}_{-0.12}$
χ^2_ν	1.24 (17 dof)

2.4.2. *Line Features and Hard Tail*

Ohashi et al. (1989) went into some detail searching for spectral features in their analysis of the 1987 May *Ginga* observation of the source. In summary, these authors found no evidence for any spectral features beyond a simple power law with low-energy absorption over the energy range 1.7 to 35 keV. It should be noted that these authors fixed the column density at a relatively high value of $N_H = 1.3 \times 10^{21}$ cm^{-2} which may account for their nondetection of the low-energy spectral break. Upper limits at 90% confidence of 50 eV for the equivalent width of an Fe K_α emission line and 2×10^{17} cm^{-2} for the column density of an Fe K_α absorption edge were derived. The presence of a hard tail was also tested for by fitting these data with a multiple component model consisting of two power laws. The hard tail was modelled by fixing the photon index of one power law at a value of zero. An upper limit at 90% confidence of 0.3 μJy at 20 keV for the intensity of this component was obtained.

We have repeated this exercise using a statistically well constrained spectrum obtained by integrating a subset of the 1989 October 2 data from time bins 7 to 15 (see Fig. 2). During this time the background rate within the detectors was at a minimum due to relatively *shallow* passages of the satellite through the SAA. A broken power-law model, with low energy absorption fixed at the Galactic value was first fit to these data. This model provides a good fit with the minimum $\chi^2_\nu = 1.28$ for 40 degrees of freedom. The best-fit spectral parameters were, $\alpha_{low} = 1.40^{+0.04}_{-0.06}$, $\alpha_{high} = 1.601 \pm 0.013$ and $E_{break} = 3.24 \pm 0.34$ keV (errors are 68% confidence intervals assuming three parameters of interest). The break energy is within two standard deviations of the mean break energy found earlier and $\alpha_{low} \simeq \alpha_{high} - 0.2$. The incident photon spectrum and residuals of the fit are shown in Figure 8. The addition of an emission line fixed at an energy of 5.8 keV and an edge fixed at an energy of 6.4 keV (6.4 keV and 7.1 keV, respectively, in the rest frame of the source) did not significantly improve on the fit and upper limits at 90% confidence of 34 eV for the line equiv-

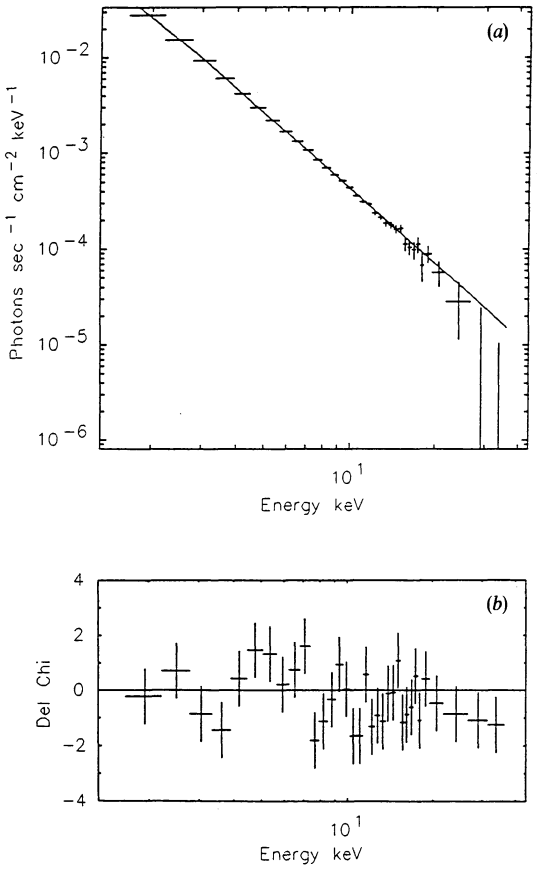

FIG. 8.—(*a*) Incident photon spectrum for the 1989 October 2 data and the best-fit broken power-law model fitted to the data. (*b*) Residuals of the fit in units of $\Delta\chi^2$.

alent width and 9.8×10^{17} cm^{-2} for the edge column density were derived. The confidence limits were calculated assuming three parameters of interest in the fit. As we have previously demonstrated the low-energy curvature has a fixed relation with the high-energy slope so we have effectively one parameter of interest resulting from the broken power-law component to the model (the source intensity is not a strong function of the remaining spectral parameters) and two parameters of interest from the line intensity and edge column density.

There is no evidence for a hard tail component in this spectrum and, if anything, the spectrum appears to steepen further above 15 keV. We derived an upper limit at 90% confidence of 0.05 μJy at 20 keV for the intensity of the hard tail component. The intensity of the hard tail measured with *HEAO 1* A-2 was 0.8 ± 0.2 μJy which is well above the upper limits derived in this work and by Ohashi et al. (1989). The ratio of the predicted synchrotron and self-Compton X-ray fluxes is model dependent and extremely sensitive to the source parameters. For example, in the simplest homogeneous SSC model with the emission region moving relativistically at some angle to the line of sight the self-Compton flux is proportional to the kinematical Doppler factor raised to a high power. Hence it is feasible that a small change in the physical condition of the source could have enhanced the self-Compton component during the *HEAO 1* observation relative to the later *EXOSAT* and *Ginga* observations.

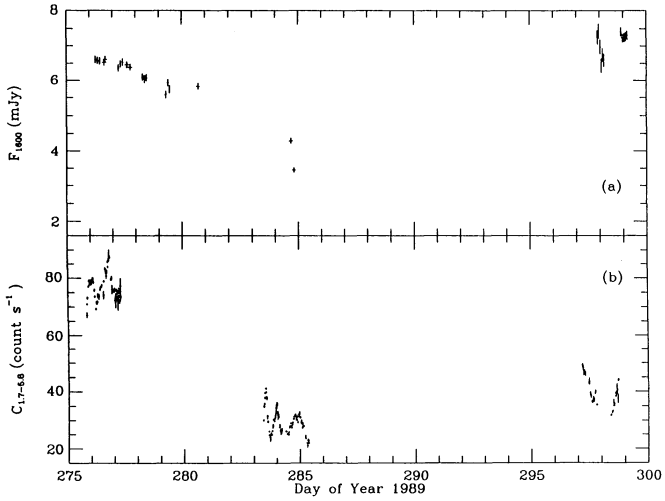

FIG. 9.—Flux density at 1600 Å (*upper panel*) and 1.7–5.8 keV count rate (*lower panel*) vs. time.

3. COMPARISON WITH COMTEMPORANEOUS ULTRAVIOLET OBSERVATIONS

During 1989 October PKS 2155−304 was also the subject of an extensive series of observations by *IUE* (Edelson et al. 1991). Most of these observations were contemporaneous with the *Ginga* observations reported in this paper. Thirty spectra were obtained by the short-wavelength camera (SWP) and 27 by the long-wavelength camera (LWP). No correlation between spectral slope and flux was observed in the LWP, however, a possible weak dependence was seen in the SWP (see also Maraschi et al. 1986) in the sense that the slope is harder when the continuum is brighter.

In Figure 9 we have plotted the flux at 1600 Å (from the SWP observations) along with the 1.7–5.8 keV *Ginga* light curves (Figs. 2*a*, 3*a*, and 4*a*). In both wavebands the source reached its faintest level on October 10–12 following a marked decline in the flux from the October 3 period (by a factor ~ 2 in the ultraviolet and ~ 3 in the X-ray regime). However, by October 24 the source had reached its maximum intensity in the ultraviolet whereas in X-rays it was still a factor ~ 2 below its October 3 high state. This corresponds to a gradual steepening of the broad band ultraviolet to X-ray (1600 Å–2 keV) energy index α_{ux} from ~ 0.93 on October 3 to ~ 1.05 on October 24 (see Table 3). Unfortunately, short time scale variability of the magnitude evident in the X-ray light curves is near the limit of that detectable in the *IUE* observations, although fairly rapid changes in the ultraviolet flux are apparent on October 11 and October 25. Given the rather limited simultaneous coverage little can be concluded about the correlation between ultraviolet and X-ray fluxes on the time scale of the X-ray flaring activity.

TABLE 3

MEAN *Ginga* AND *IUE* SWP SPECTRAL PARAMETERS IN 1989 OCTOBER

Date	S_{uv} (mJy)	S_x (mJy)	α_x	α_{ux}	S_B (mJy)	E_b (keV)
1989 Oct 2	6.6	0.122	1.45	0.93	0.38	0.45
1989 Oct 10	3.8	0.054	1.60	0.99	0.25	0.39
1989 Oct 24	7.0	0.074	1.63	1.05	0.55	0.29

During this period the source was also observed in the optical waveband (Carini & Miller 1992). Between October 3 and October 8 the V-band flux decreased by $\sim 11\%$. Hence, within the limits of the sparsity of the data, the continuum from optical to X rays would appear to be roughly correlated on a time scale of weeks. This behavior was also observed on a longer time scale during a multiwavelength campaign over nine epochs from 1983 to 1985 by Treves et al. (1989).

4. DISCUSSION

The multiwavelength continuum of BL Lac objects is most commonly interpreted in terms of nonthermal emission, such as synchrotron or synchrotron self-Compton (SSC) radiation, produced within a highly anisotropic, and possibly relativistically beamed, geometry (see e.g., Hutter & Mufson 1986; Urry 1988, and references therein). In their simplest form these models require the observed continuum to arise solely from a jet extending outwards from the central engine along an axis perpendicular to the preferred plane of angular momentum transport within the nucleus. Such models can explain with reasonable success the overall smoothness of the continuum, the rapid variability and the polarization properties of many BL Lac objects, provided the angle between the line of sight of the observer and the jet axis is small.

In an alternative approach, Wandel & Urry (1991) have suggested that the ultraviolet to soft X-ray emission from PKS 2155−304 may originate from thermal radiation from a cool accretion disk. They further speculate that the hard X-ray emission may arise from the Comptonization of the thermal seed photons by a hot corona above the disk. In such a scenario the hard X-ray emission is fairly isotropic and hence $\sim 50\%$ of the hard X-ray photons will illuminate the cool disk. Some fraction of this radiation will be reprocessed as an Fe K_α emission line. George & Fabian (1991) have calculated the expected equivalent width of this line for a cool disk illuminated by a centrally located X-ray source. The equivalent width is a function of a variety of parameters, the most important being the inclination of the disk, the total fraction of the radiation field incident on the disk, and the power-law index of the continuum. In the case of a face-on disk illuminated by an isotropic X-ray flux with $\alpha \simeq 1.6$ an equivalent width of ~ 100 eV is expected, whereas for PKS 2155−304 we obtain an upper limit of 34 eV for the equivalent width of such a line. To bring the predicted line equivalent width within the observed limit would require either the inclination angle of the disk to be greater than 80° (i.e., edge on) or the X-ray emission to be anisotropic and that the observer sees a much greater fraction than the disk. In the former case a highly inclined disk would naturally imply that any jets directed out from the nucleus would then be almost perpendicular to the line of sight and, irrespective of the physical mechanism behind the X-ray emission, would contradict the observed radio to optical properties of the source. In the latter case the need for anisotropic X-ray emission somewhat undermines the need for a disk and naturally leads one back to some form of jet model.

In jet models, the X-ray emission can arise as either direct synchrotron radiation or from inverse Compton scattering of the softer synchrotron photons by the relativistic electron population. In fact, it may be possible to divide BL Lac objects into two classes depending on which mechanism is applicable. In PKS 2155−304 extrapolations of the flat optical to ultraviolet continuum and steep X-ray continuum meet in the soft X-ray band. This spectral form is suggestive of the direct synchrotron origin with the spectral break being attributable to radiation losses suffered by the electron population. In the archetype of the class, BL Lacertae, the inverse Compton origin is more likely because the X-ray spectrum is flatter than in the optical-ultraviolet with a slope similar to the millimeter-infrared continuum which may provide the seed photons (Bregman et al. 1990).

It is interesting to compare the spectral properties of PKS 2155−304 with other X-ray bright BL Lac objects which have a similar multiwaveband spectrum. *EXOSAT* and *IUE* observations of Mrk 501, Mrk 180, PG 1218+304 (George, Warwick, & McHardy 1988), and Mrk 421 (George et al. 1988) taken over time scales of weeks to months, show that the steep X-ray continuum is more rapidly variable than the flatter ultraviolet continuum with the X-ray spectra showing a clear tendency to harden as the continuum level increases. For the sources noted above the spectral variability gave rise to a behavior which can be modelled in an empirical fashion by assuming that the X-ray continuum was pivoting about a fixed break point at an energy of ~ 0.1 keV.

Table 3 summarizes the results of applying this empirical description to PKS 2155−304. We have estimated the break point in the X-ray to ultraviolet continuum for each of the 1989 October observations as the point at which the extrapolated ultraviolet spectrum (assuming a fixed value $\alpha_{uv} = 0.7$) and the mean X-ray spectrum below the break at ~ 4 keV intersect. Table 3 lists the mean *IUE* flux at 1600 Å, the mean X-ray flux at 2 keV, the mean X-ray spectral index in the 1.7 to 3.8 keV range, the mean ultraviolet to X-ray index, together with the flux and energy (f_b, E_b) of the inferred break point. We have excluded the soft flare events evident in the *Ginga* data during 1989 October 2 and 1989 October 24. The inferred break point is at ~ 0.3–0.4 keV which is at a somewhat higher energy than that estimated for the BL Lac objects discussed above. Over the October period there is an indication that the break point was gradually moving to lower energies (essentially an alternative description to the net steepening of α_{ux} noted earlier). Figure 10 shows the three tracks which are obtained in the index-flux plane assuming the spectra pivot at the break points given in Table 3. The tracks provide a remarkably good fit to the data considering the somewhat ad hoc method of deriving the break point parameters.

These results suggest that the majority of the variations in the ultraviolet to X-ray continuum of PKS 2155−304 can be explained by two factors. First, the whole continuum can rise or fall with a correlation of the hardness of the X-ray slope with intensity on time scales of a week or greater. Second, rapid variations within the X-ray band occur on time scales down to a few hours which can be parameterized by assuming that the spectrum pivots about a break point ~ 0.3–0.4 keV.

Variability of the first type has been modeled by Celotti, Maraschi, & Treves (1991) who have calculated the time-dependent spectral properties arising from a perturbation of the synchrotron emissivity travelling at a fixed speed down the axis of a jet. Below the break frequency of the stationary jet, the spectral slope remains constant whereas at higher frequencies the slope hardens with increasing intensity. Variability of the second type has been considered by George et al. (1988) who have shown that if the maximum energy of the synchrotron emitting electrons, and hence the maximum emitted frequency, has a radial dependence then the observed X-ray spectral index can be shown to be a function of the parameterization of the upper cutoff in the electron energy distribution whereas the

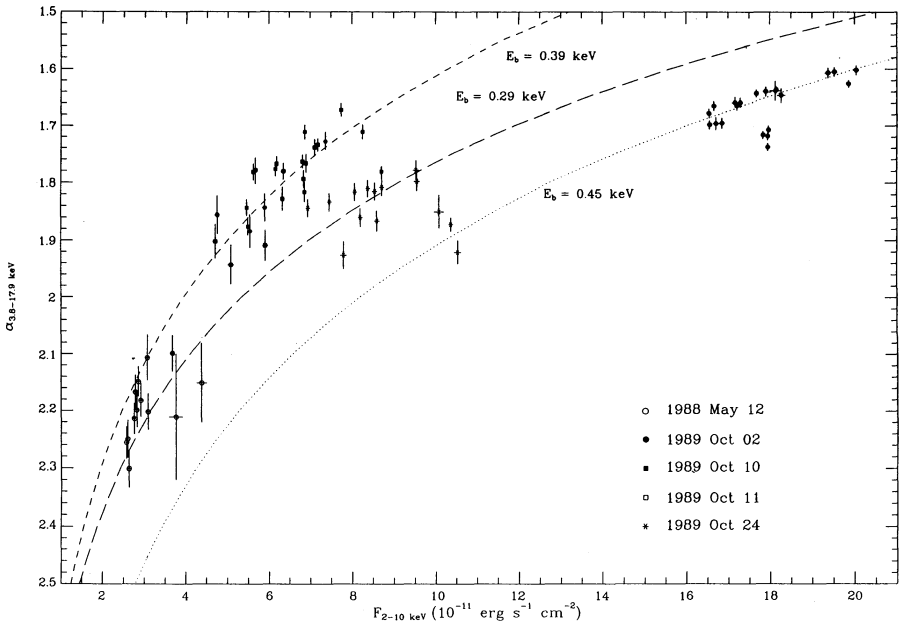

FIG. 10.—Best fit spectral index in the range 3.8–17.9 keV plotted against absorption corrected 2–10 keV flux for the two parameter fits. Also plotted are the tracks corresponding to the expected relation between index and flux for the break parameters given in Table 3.

spectrum at longer wavelengths is not. Temporal variations in the efficiency of the re-acceleration process within the X-ray emitting region could therefore provide a plausible physical mechanism for some of the rapid X-ray variability.

Of course this picture fails to explain some of the observations in detail; namely the soft flare events (assuming that they are not due to a serendipitous source) and the apparent complex relation between flux and index during the rise and decays phases of the 1989 October 10/11 data. In most jet models the X-ray emitting region covers a range of radii and a continuous range of magnetic field strengths and particle densities. However, because of the need for in situ electron re-acceleration processes the jet may contain compact regions, or knots, possibly associated with shock fronts, which can produce variability in the observed X-ray emission independently of the remaining X-ray emitting region. Hence, a possible origin for the soft flare event may then be a knot in the inhomogeneous jet whose local physical conditions were somewhat different to the surrounding jet region at that time. Perhaps the most interesting observation is that of the relationship between index and intensity in the 1989 October 10/11 data. The *clockwise* looping of the index-flux points in parameter space during the rise and decay phases is consistent with simple synchrotron emission processes if the time scale for flux variability is more rapid than the time scale for the electron population to reach equilibrium; in this case, since the time scale for synchrotron losses is faster for higher energy electrons when the flux rises or decays, the hard X-ray photons respond faster than the soft X-ray photons. This may explain why the rise and decay phase of the much longer second 1989 October 2 flare follows the same track in index-flux parameter space.

In conclusion, the high-quality *Ginga* data presented here have shown that the time-dependent spectral evolution of PKS 2155−304 is complicated with multiple modes of behavior over the period of the observations. This implies that there are probably a variety of physical processes which give rise to the observed variability properties. Not only is there an obvious need for more detailed time-dependent models within the literature, there is an even more pressing need for future X-ray monitoring observations of BL Lacertae objects to be coordinated with observations at lower frequencies despite the inherent difficulties of organizing such campaigns.

The authors would like to thank the members of the *Ginga* Team in Japan and the UK for their invaluable support work. C. M. U. and T. O. thank the STSCIC visitor program under whose auspices some of this work was carried out. C. M. U. and J. S. acknowledge the support of NASA grant NAG 8-697. I. M. G. acknowledges support from the Universities Space Research Association (USRA).

REFERENCES

Blandford, R. D., & Rees, M. J. 1978, in Pittsburgh Conf. BL Lac Objects, ed. A. M. Wolfe (Pittsburgh: Univ. Pittsburgh), 328
Bowyer, S., Brodie, J., Clarke, J. T., & Henry, J. P. 1984, ApJ, 278, L103
Bregman, J. N., et al. 1990, ApJ, 352, 574
Canizares, C. R., & Kruper, J. 1984, ApJ, 278, L99
Carini, M. T., & Miller, H. R. 1992, ApJ, 385, 146
Celotti, A., Maraschi, L., & Treves, A. 1991, ApJ, 377, 403
Edelson, R. A., et al. 1991, ApJ, 372, L9
Falomo, R., Giraud, E., Maraschi, L., Melnick, J., Tanzi, E. G., & Treves, A. 1991, ApJ, 380, L67
Falomo, R., Melnick, J., & Tanzi, E. G. 1990, Nature, 345, 692
George, I. M., & Fabian, A. C. 1991, MNRAS, 249, 352
George, I. M., Warwick, R. S., & Bromage, G. E. 1988, MNRAS, 232, 793
George, I. M., Warwick, R. S., & McHardy, I. M. 1988, MNRAS, 235, 787
Giommi, P., Barr, P., Garilli, B., Maccagni, D., & Pollock, A. M. T. 1990, ApJ, 356, 432
Griffiths, R. E., Tapia, S., Briel, U., & Chaisson, L. 1979, ApJ, 234, 810
Hayashida, K., et al. 1989, PASJ, 41, 373
Hutter, D. J., & Mufson, S. L. 1986, ApJ, 301, 50
Kellerman, K. I. 1966, ApJ, 146, 621
Krolik, J. H., Kallman, T. R., Fabian, A. C., & Rees, M. J. 1985, ApJ, 295, 104
Madejski, G., et al. 1991, in 28th Yamada Conf. Frontiers of X-ray Astronomy, ed. Y. Tanaka & K. Koyama (Tokyo: Universal Academy Press), 583
Maraschi, L., Tagliaferri, G., Tanzi, E. G., & Treves, A. 1986, ApJ, 304, 637

Morini, M., Chiappetti, L., Maccagni, D., Maraschi, L., Molteni, D., Tanzi, E. G., Treves, A., & Wolter, A. 1986, ApJ, 306, L71
Morrison, R., & McCammon, D. 1983, ApJ, 270, 119
Ohashi, T., Makishima, K., Inuoue, H., Koyama, K., Makino, F., Turner, M. J. L., & Warwick, R. S. 1989, PASJ, 41, 709
Pallavicini, R., Tagliaferri, G., & Stella, L. 1990, A&A, 228, 403
Schwartz, D. A., Doxsey, R. E., Griffiths, R. E., Johnston, M. D., & Schwartz, J. 1979, ApJ, 229, L53
Tagliaferri, G., Stella, L., Maraschi, L., Treves, A., & Celotti, A. 1991, ApJ, 380, 78
Treves, A., et al. 1989, ApJ, 341, 733
Turner, M. J. L., et al. 1989, PASJ, 41, 345
Urry, C. M., & Mushotzky, R. F. 1982, ApJ, 253, 38
Urry, C. M., Mushotzky, R. F., & Holt, S. S. 1986, ApJ, 305, 369
Urry, C. M., et al. 1992, in preparation
Wandel, A., & Urry, C. M. 1991, ApJ, 367, 78